Mathematical Modeling of a Bioluminescent
E. Coli Based Biosensor

A. Rabner[1], **E. Martinez**[2], **R. Pedhazur**[3], **T. Elad**[3], **S. Belkin**[3], **Y. Shacham**[1]

[1]Physical Electronics Department, Tel-Aviv University, Ramat-Aviv, Tel-Aviv 69978, Israel
arthur.rabner@gmail.com

[2]Biomedical Engineering Department, Tel-Aviv University, Ramat-Aviv, Tel-Aviv 69978, Israel

[3]Department of Plant and environmental Sciences, Hebrew University of Jerusalem
Jerusalem 91904, Israel

Abstract. In this work we present a mathematical model for the bioreporter activity of an *E. coli* based bioluminescent bioreporter. This bioreporter is based on a genetically modified *E. coli* which harbors the recA promoter, a member of the bacterial SOS response, fused to the bacterial luminescence (*lux*) genes. This bioreporter responds to the presence of DNA damaging agents such as heavy metals, H_2O_2 and Nalidixic Acid (NA) that activate the SOS response. In our mathematical model we implemented basic physiological mechanisms such as: the penetration of the NA into the biosensor; gyrase enzyme inhibition by the NA; gyrase level regulation; creation of chromosomal DNA damage; DNA repair and release of ssDNA into the cytoplasm; SOS induction and chromosomal DNA repair; activation of *lux* genes by the fused *recA* promoter carried on a plasmidal DNA; transcription and translation of the luminescence responsible enzymes; luminescence cycle; energy molecules level regulation and the regulation of the O_2 consumption.

The mathematical model was defined using a set of ordinary differential equations (ODE) and solved numerically. We simulated the system for different concentrations of NA in water for specific biosensors concentration, and under limited O_2 conditions. The simulated results were compared to experimental data and satisfactory matching was obtained. This manuscript presents a proof of concept showing that real biosensors can be modeled and simulated. This sets the ground to the next stage of implementing a comprehensive physiological model using experimentally extracted parameters. Following the completion of the next stage, it will be possible to construct a "Computer Aided Design" tool for the simulation of the genetically engineered biosensors. We define a term "bioCAD" for a Biological System Computer Aided Design. The specific bioCAD that is described here is aimed towards whole cell biosensors which are under investigation today for functional sensing. Usage of the bioCAD will improve the biosensors design process and boost their performance. It will also reduce Non Recurring Engineering (NRE) cost and time. Finally, using a parameterized solution will allow fair and quick evaluation of whole cell biosensors for various applications.

Keywords: bioluminescence, enzymes, biosensor, promoting, reporting, photons, luciferase, aldehyde, fatty acid.

1 Introduction

Today, the design of biosensors does not include a computer based simulation stage as a standard procedure similar to what was a standard use in most engineering disciplines. The current commonly-practiced "trial and error" method which is used for biosensor design is a complex, expensive and time-consuming process that fails to guarantee the required system performance. Therefore, currently there is a need for a computer aided design (bioCAD) tool for biosensor engineering.

Any CAD tool is based on mathematical modeling of the resources and processes of the corresponding object. The bioCAD for the whole cell biosensors engineering has to cope with cellular functions that are based on a large number of chemical reactions and transport processes that are regulated by proteins, enzymes, genetic and biomechanical mechanisms [1–4]. The relatively simple mathematical models deal with enzymes and substrates by ordinary differential equations (ODE) [5–8]. A more sophisticated form, considering diffusion, is based on the partial differential equation (PDE), as shown for example in works describing a biosensor acting in a trigger mode [9] and in the *Vibrio fisheri* control system [10]. The genetic and biomechanical mechanisms could be found in works depicting the *E. coli* SOS function [11–13] for damaged DNA repair. The modeling could be stochastic or deterministic, depending on a number of substrate and reactant molecules [14–16] that are being taken into consideration.

Metabolism is commonly defined as a process in which nutrients are converted to provide energy and the synthesis of new organic materials for the cells maintenance activity and reproduction [17, 18]. Therefore, metabolism modeling usually appears in most whole cell biosensors [16]. This modeling is usually very complex and it is common to derive algorithms for simplifying the metabolic networks [6, 19, 20]. The second major issue is the modeling of the regulatory networks. For example, those were comprehensively studied and modeled for *E. coli* [6, 16, 19, 21], and for *Synechocystis* [22].

The other main parts of the biosensor mathematical model are: (i) the interaction of the analyte with the biosensor; (ii) the biosensor response; and (iii) the reporting mechanisms. The analyte interaction with the biosensor, which is the initial link in the detection chain of the bioreporter, has been reviewed in the literature, for example see references [23, 24]. The biosensor response activates the reporting mechanism. The SOS mechanism (a response tool for the repair of a DNA damaged by the analyte) is described in a variety of works [11–13, 25, 26]. Other response mechanisms models are based on transcription of signaling proteins and enzymes [27, 28]. In our research we are investigating luminescent bioreporters that are based on the activation of bacterial luminescence genes (*lux*) derived from marine luminescent bacteria *Vibrio fisheri*, all of them are well-studied mechanisms [29–32].

We use "normally-off" *E. coli* based bioluminescence biosensors incorporated into 1–100 μL reaction chambers, densely packed on a biochip. Special μFluidics on the biochip are used for translocation of the tested liquid with different concentrations of Nalidixic Acid (NA) into the reaction chambers. O_2 supply, which is vital for bacterial metabolism and for bioluminescence, is relatively limited. The absence of excess O_2 supply makes the biosensors environment "unfriendly" and limiting the light generation

efficiency.

The implementation of Stage-I of the biosensor Computer Aided Design (bioCAD) roadmap, see Fig. 1, is demonstrated in this work. The roadmap consists of three stages. The Stage-I is for bioCAD proof of concept for the whole cell *E. coli* based bioluminescent biosensor. Only the main physiological processes are used in Stage-I. In this stage most of the reaction and process parameters are taken from the literature or, alternatively, assumed by some intelligent guess which is appropriate to the physiological mechanism. The simulated biosensor behavior matches in general the kinetics from the experimental results and therefore lays the ground to Stage-II.
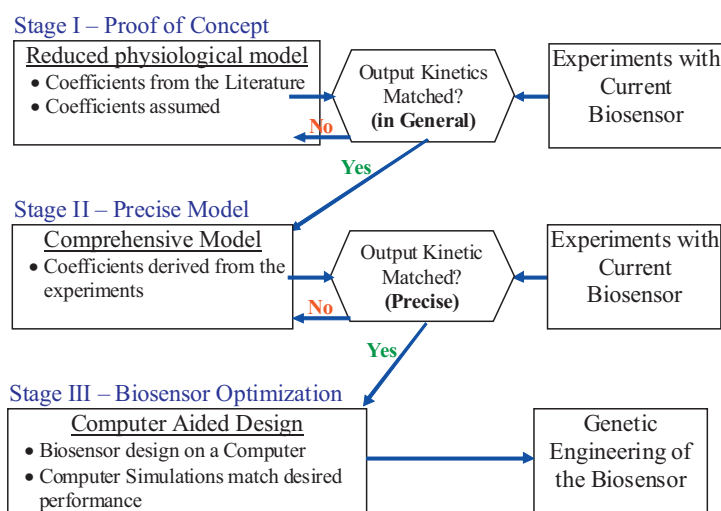
Fig. 1. Stages for development of computer aided design for bioluminescent *E.Coli* based biosensor.

During Stage-II of the roadmap (Fig. 1), the mathematical model should be expanded to a "Comprehensive Physiological Model" while the parameters should be experimentally measured for the specific biosensor used in the research. For the successful completion of this stage the simulation should match exactly the experimental behavior. Once completed, the model could be used for the computer aided design to improve the biosensor performance which is the main part of Stage-III (see Fig. 1).

There is a diversity of factors that could be desired to boost the performance of the biosensor. Here a few are mentioned: (i) shortening the response time between the analytes incursion and the reporting initiation; (ii) increasing the reporting intensity; (iii) defining a selective response for specific analytes; (iv) adjusting the amplitude of the reporting response corresponding to the analytes concentration, etc. Design and simulation of the new biosensor will tremendously reduce the demands for time, labor and financial resources. Once the desired performance is met, the actual biosensor can

be built and applied. Next, the bio sensor's experimental behavior should be compared to that of the simulation, and the difference between them should be studied. A good model will yield a reasonable match, yielding a working functional biosensor applicable for system interfacing. Under other circumstances, it is necessary: (a) to check the physical implementation of the biosensor and (b) to check the comprehensive physiological model and repeat the evaluation process until the matching is achieved.

In this section we have presented a diversity of work dealing with modeling of various biological processes. However, the complete physiological model of genetically engineered biosensor based on *E. coli*, SOS response and luminescence reporting has not been implemented yet. In the current work we did such an implementation, successfully validated it, and now it is possible to proceed with the 2nd step toward biosensor computer aided design development.

2   Biosensor mathematical model

In this work we build the complete model of a genetically engineered bioluminescent *E. coli* based biosensor using subsets of equations describing the critical physiological mechanisms. Note that, as described before, only to the conceptual model is referred to, where only the rate defining steps are taken into consideration. Simplified models for those steps have been used.

Those mechanisms are (i) analyte uptake and SOS response; (ii) simplified metabolism regulation model; (iii) simplified O_2 consumption; and (iv) light generation process. All the aforementioned mechanisms have mutual dependency creating a network or a biological feedback circuit. Activation of each mechanism depends also on the physiological state of the biosensor. The physiological states of the biosensor are described in the following sub-section.

2.1   Biosensor's physiological states

The biosensor under investigation referrers to bacteria that are positioned within reactions chambers on a chip. In this case the biosensors are typically enclosed within porous polymer matrix, such as oxide Sol-Gel or agar, and we may assume that mitosis is prohibited. Therefore, the possible main physiological states are as shown in Fig. 2.
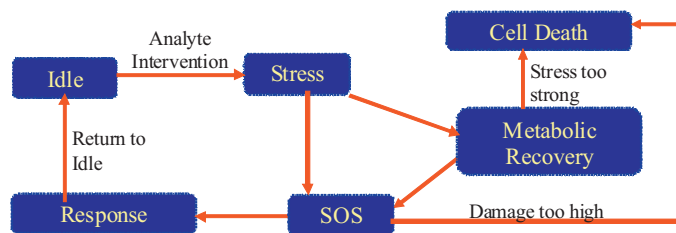
Fig. 2. Physiological states of the biosensor.

Initially the biosensor is in an "Idle State". Once analytes are introduced, the internal machinery of the biosensor is damaged and it becomes under a "Stress" condition. Following the stress, the sensor enters into a "Recovery State". In our particular case the stress is actually DNA damage and hence the "Recovery State" is combined of two processes: (i) a SOS response and (ii) a "Metabolic Recovery". If the stress induced injury is above some threshold level the cell dies, i.e. enters the "Cell Death State". Otherwise it generates a reporting response, i.e. enters the "Response State". The processes of stress, metabolic recovery and SOS, could continue while the sensor is in the "Response State". Once the stress and the recovery processes are completed the sensor returns to the "Idle State".

2.2 Analytes uptake dynamics and SOS response activation

In this section the process of analyte uptake by the biosensors and the activation of the SOS response are shown. First the problem is reduced to a single biosensor. The model simplification is achieved by assuming uniform distribution of the biosensors and analytes inside the reaction chamber. Each biosensor is treated as a "reaction center" as demonstrated in Fig. 3.
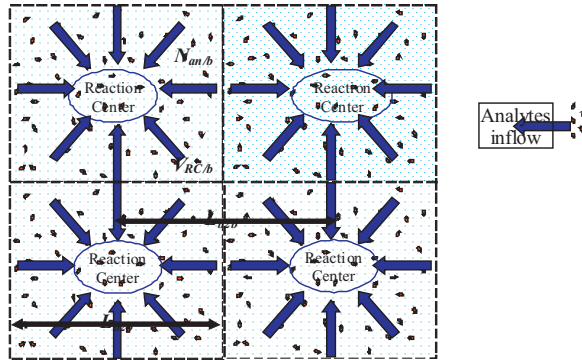
Fig. 3. Partitioning of the reaction chamber for "Per Bacterium" sub-volumes.

Assuming a reaction chamber with volume V_{RC} and the biosensor concentration of C_b, the number of the biosensors inside the reaction chamber N_b is:

$$N_b = V_{RC} \cdot C_b. \tag{1}$$

We also assume that the average volume of reaction chamber for single biosensor, $V_{RC/b}$ is:

$$V_{RC/b} = V_{RC}/N_b = 1/C_b. \tag{2}$$

In this case, the average distance, L_{b2b}, between two adjustment biosensors is:

$$L_{b2b} = \sqrt[3]{V_{RC/b}}. \tag{3}$$

We assume that the concentration of the introduced analyte is uniform through the reaction chamber and each biosensor, in average, shares the same amount of the analyte molecules. The analytes concentration, C_{an-ppm}, is given in "parts per million" (ppm) that is equivalent to mg/L. The average number of analyte molecules $N_{an/b}$ per partition sub-volume, $V_{RC/b}$ is given by:

$$N_{an/b} = \frac{C_{an-ppm}}{1000 \cdot MW_{an}} \cdot V_A \cdot V_{RC/b} = \frac{C_{an-ppm}}{1000 \cdot MW_{an}} \cdot V_A \cdot 1/C_b, \qquad (4)$$

where MW_{an} is a molecular weight of the analyte and N_A is an Avogadro number. For example, for 1 ppm of Nalidixic Acid (NA) with $MW_{NA} = 232$ gr/mole, reaction chamber with volume $V_{RC} = 1\ \mu$L, biosensors concentration $C_b = 5e5$ b/μL, the number of the NA molecules per volume of reaction chamber utilized by a single bacterium is:

$$N_{an/b} = \frac{1}{1000 \cdot 232} \cdot 6 \cdot 10^{23} \cdot \frac{1}{5 \cdot 10^5 \cdot 10^6} = 5.17 \cdot 10^6 \text{ Molecules}.$$

The Nalidixic Acid (NA) analyte emulates a group of toxicants that damages the chromosomal DNA of the bacterium. Note that NA is relatively safe for humans and, therefore, preferably used to test the performance of such biosensors; consequently we selected using NA in our work. The simplified scheme of the NA uptake and SOS process activation is depicted in Fig. 4.
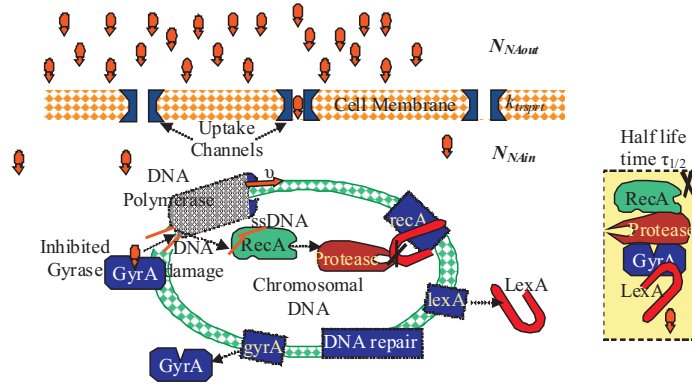
Fig. 4. NA uptake and chain reactions of the SOS process initialization.

We assume that the analyte transport in the liquid (free or enclosed in a porous matrix), via diffusion or convection, is not the rate determining factor. For example, taking the data in the abovementioned test case, the average dimension of the reaction chamber volume utilized by the biosensor is $L_{b2b} = \sqrt[3]{1/C_b} = \sqrt[3]{1/(5 \cdot 10^5 \cdot 10^6)} \cdot 10^5 = 12.6\ \mu$m. The diffusion coefficients of most water-soluble compounds with low molecular mass are in the order of $D \sim 1e-5$ cm^{2}s^{-1} [24]. Therefore, the average diffusion time

of such molecules, t_{b2b} is

$$t_{b2b} \approx \frac{(L_{b2b}/2)^2}{D} = 0.15 \text{ sec.} \tag{5}$$

The uptake rate of the analyte like NA is faster in few orders of magnitudes than the resulted reaction (0.15 sec versus minutes). Therefore, the transport of analytes like NA is not limited by diffusion and it is not taken into consideration. The analytes penetrate into the bacterium through uptake channels available on the membranes of the biosensor. The change of NA concentration inside the biosensor is expressed by the following equation:

$$\frac{\mathrm{d}NA_{in}}{\mathrm{d}t} = k_{trn-NA} \cdot (NA_{out} - NA_{in})$$
$$- \frac{NA_{in}}{H_{NA}} - (k_{GyrA.NA} \cdot GyrA \cdot NA_{inMolar}) \cdot (N_A \cdot V_b), \tag{6}$$

where k_{trn-NA} is a concentration gradient coefficient indicating the percentage of molecules transported through the cell membrane per second, NA_{in}, NA_{out} are the NA concentration inside and outside the biosensor correspondingly, H_{NA} is the half life time of the NA molecule degradation, $k_{GyrA.NA}$ is a constant rate of interaction between NA and gyrase enzymes whose concentration is marked by $GyrA$. We also use molar concentration, $NA_{inMolar}$ that is converted from the number of molecules per bacteria using the Avogadro number N_A and the bacterium volume V_b:

$$NA_{inMolar} = NA_{in}/(N_A \cdot V_b). \tag{7}$$

Outside the biosensor the change in NA concentration is as following:

$$\frac{\mathrm{d}NA_{out}}{\mathrm{d}t} = -k_{trn-NA} \cdot (NA_{out} - NA_{in}) - \frac{NA_{out}}{H_{NA}}. \tag{8}$$

The NA analyte inhibits the gyrase enzymes. The gyrase enzyme is responsible for unwinding supercoiled DNA during replication. However, when gyrase is attached to the DNA, but inhibited by NA, it fails to function and DNA lesion is created in that region [33]. In our model we assume that DNA polymerase enzymes repair the dimers. The repair is modeled by polymerase motion on the chromosome which causes the removal of the lesions. We will relate to the lesion's site as a "DNA dimer". Once the lesion is detached and corresponding DNA fragment is repaired, the dimer is removed. The change in the number of dimers, N_{dim}, could be expressed as:

$$\frac{\mathrm{d}N_{dim}}{\mathrm{d}t} = \frac{\mathrm{d}N_{dim-gen}}{\mathrm{d}t} - \frac{\mathrm{d}N_{dim-rep}}{\mathrm{d}t}, \tag{9}$$

where $\mathrm{d}N_{dim-gen}$ and $\mathrm{d}N_{dim-rep}$ are the number of dimers generated and repaired correspondingly. The number of the generated dimers depends on the number of inhibited gyrase enzymes $GyrA_{inh}$ attached to the chromosomal DNA ($GyrA_{inhDNA}$). The rate of damage production is expressed by means of a rate coefficient k_{dim}:

$$\frac{\mathrm{d}N_{dim-gen}}{\mathrm{d}t} = k_{dim} \cdot GyrA_{inhDNA} \cdot N_A \cdot V_b. \tag{10}$$

The concentration of the inhibited gyrase molecules attached to DNA ($GyrA_{inhDNA}$) is mediated by a constant $k_{GyrA.DNA}$, the gyrase half life time H_{GyrA} and also decreases through the dimers repair process:

$$\frac{dGyrA_{inhDNA}}{dt} = k_{GyrA.DNA} \cdot GyrA_{inh}$$
$$- \frac{GyrA_{inhDNA}}{H_{GyrA}} - \frac{dN_{dim-gen}}{dt} \cdot \frac{1}{N_a \cdot V_b}. \tag{11}$$

The change in the total number of the inhibited gyrase enzymes is a function of the NA ⇔ gyrase binding coefficient $k_{GyrA.NA}$:

$$\frac{dGyrA_{inh}}{dt} = k_{GyrA.NA} \cdot GyrA \cdot NA_{inMolar}$$
$$- \frac{GyrA_{inh}}{H_{GyrA}} - k_{GyrA.DNA} \cdot GyrA_{inh}. \tag{12}$$

The cell can regulate gyrase concentrations [34]. In our model we assume that the gyrase concentration decreases due to NA inhibition and some effect on transcription. The gyrase concentration and production rate deviates from their normal values, $GyrA_{norm}$, and $T_{GyrAnorm}$, respectively. In this case the rate of gyrase production, T_{GyrA} is accelerated. This rate is modeled by the following function of some arbitrary coefficients $GyrA_{min}$ and P_{GyrA}, and also $GyrA_{norm}$ which was described before.

$$T_{GyrA} = T_{GyrAnorm} \cdot \left(\frac{GyrA_{norm} + GyrA_{min}}{GyrA + GyrA_{min}} \right)^{P_{GyrA}}. \tag{13}$$

Next, we present the change in the gyrase concentration that depends on the gyrase production rate T_{GyrA}, the inhibition of the gyrase by the NA and the half life time H_{GyrA}:

$$\frac{dGyrA}{dt} = T_{GyrA} - k_{GyrA.NA} \cdot GyrA \cdot NA_{inMolar} - \frac{GyrA}{H_{GyrA}}. \tag{14}$$

The dimer removal rate depends on the average distance (in nucleotides) between the damaged DNA, L_{d2d}, the velocity of DNA polymerase (DNAP) movement on the DNA, v_s, and the delay, t_{dim}, that takes to repair the damaged part of the DNA:

$$\frac{dN_{dim-rep}}{dt} = 2 \cdot k_{bind} \cdot DNAP \cdot \frac{1}{t_{dim} + (L_{d2d}/v_s)}, \tag{15}$$

where the $DNAP$ is the number of DNA polymerase enzymes in a cell and k_{bind} is a binding probability of those enzymes to the chromosomal DNA. The coefficient 2 that appears in equation (13) is due to the two replication forks that are moving in opposite directions at similar rates. The average distance between two dimers is a ratio between

the lengths in nucleotides of chromosomal DNA (L_{ChrDNA}) to the current number of dimers:

$$L_{d2d} = L_{ChrDNA}/N_{dim}. \tag{16}$$

The DNA repair process or SOS response detaches the damaged DNA parts. As a result, ssDNA fragments are released to cytoplasm. The RecA molecules that are normally under stable, low concentration bind the ssDNA fragments and are transformed into protease enzymes with constant rate $k_{protease}$. The protease enzymes interacting with LexA proteins cause the autodigestion of LexA with a constant rate k_{LexA}. The LexA protein is a direct repressor of the $lexA$ and $recA$ genes therefore the rate of synthesis of the LexA and RecA proteins is proportional to the DNA template of the $lexA/recA$ locus that is free from the repressor [11]. In the absence of the repressor, the LexA production rate is T_{LexA} and the RecA production rate is T_{RecA}, while EK_{LexA} and EK_{RecA} are the corresponding equilibrium constants. The changes in the concentrations of the $ssDNA$, $Protease$, $LexA$ and $RecA$, considering the H_{ssDNA}, $H_{Protease}$, H_{LexA} and H_{RecA} half life time constants, are expressed by a set of the following equations:

$$\frac{\mathrm{d}ssDNA}{\mathrm{d}t} = \frac{\mathrm{d}N_{dim-rep}}{\mathrm{d}t} - k_{protease} \cdot RecA \cdot ssDNA$$
$$- \frac{ssDNA}{H_{ssDNA}} + \frac{Protease}{H_{Pr-dcmp}}, \tag{17}$$

$$\frac{\mathrm{d}Protease}{\mathrm{d}t} = k_{protease} \cdot RecA \cdot ssDNA - \frac{Protease}{H_{Pr-dcmp}} - \frac{Protease}{H_{Protease}}, \tag{18}$$

$$\frac{\mathrm{d}LexA}{\mathrm{d}t} = \frac{T_{LexA}}{1 + EK_{LexA}} - k_{LexA} \cdot LexA \cdot Protease - \frac{LexA}{H_{LexA}}, \tag{19}$$

$$\frac{\mathrm{d}RecA}{\mathrm{d}t} = \frac{T_{RecA}}{1 + EK_{RecA} \cdot LexA} - k_{protease} \cdot RecA \cdot ssDNA$$
$$- \frac{RecA}{H_{RecA}} + \frac{Protease}{H_{Pr-dcmp}}. \tag{20}$$

We just have shown the SOS process where the kinetics of the $LexA$ protein concentration depends on the Nalidixic Acid analyte inducer concentration (C_{an-ppm}). Later we show how the $LexA$ level influences the intensity of the bioluminescence.

2.3 Metabolism as a function of DNA damage

We found, experimentally, that upon exposure to NA concentration above a certain level, the initial (background) luminescence activity decreases. Our assumption is that the DNA damage, that initiates the SOS process, also disturbs the rate of normal-baseline metabolism. This baseline metabolism is also responsible for the generation of reducing power and energy molecules like ATP, FMNH2 and NADPH, which we will refer to as $ENRG$, (Fig. 5).
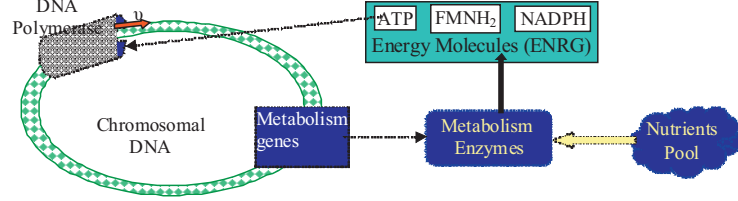
Fig. 5. Energy molecules and DNA polymerase velocity regulation scheme.

In our model we express the ENRG concentration as a function of the number of dimers N_{dim} using the following arbitrary fitting function:

$$ENRG = ENRG_{norm}\left(\frac{1}{1 + N_{dim}}\right)^{P_{dim}}, \tag{21}$$

where, P_{dim} is a fitting coefficient. The ATP, FMNH2 and NADPH are also necessary for the light generation process. The ATP is also a driving force for the DNA polymerase. Therefore, the decrease in ENRG concentration is also reflected in the velocity of DNA polymerase movement on the DNA also expressed using arbitrary fitting function:

$$v_s = v_{s-max}\left(\frac{ENRG}{ENRG_{norm}}\right)^{P_{ENRG-v}}, \tag{22}$$

where P_{ENRG-v} is a fitting coefficient and v_{s-max} is the maximal DNA polymerase velocity. The DNA polymerase promotion velocity influences the rate of DNA repair and ssDNA generation, as described in the SOS section.

2.4 Molecular oxygen consumption

The biosensors described in the current work are encapsulated into the reaction chambers of the biochip [35]. In the current system configuration, the biochip is sealed and therefore a constant oxygen supply is not obtainable. The only the available oxygen for the reaction is present in the sample to be analyzed. Normal concentration of dissolved oxygen in water is CO_2 given in [mg/L] units. It corresponds to molar concentration of:

$$C_{O_2-Molar} = C_{O_2}/MW_{O_2}, \tag{23}$$

where, MW_{O_2} is a molecular weight of the molecular oxygen. The number of the O_2 molecules per liter, N_{O_2-ltr} is:

$$N_{O_2-ltr} = C_{O_2-Molar} \cdot N_A \tag{24}$$

and the number of the O_2 molecules per bacterium is:

$$N_{O_2-b} = N_{O_2-ltr}/C_b, \tag{25}$$

We assume that O_2 freely diffuse through the bacterial membranes inside and therefore the internal O_2 concentration is equal to that of the medium of the reaction chamber. The oxygen consumption by bacterium in an aerobic condition is K_{O_2-mol}, [36] where it is expressed in [moles/min/cell] units. We transform this into [molecules/sec/cell] units and get K_{O_2norm}:

$$K_{O_2norm} = (K_{O_2-mol} \cdot N_A)/60. \tag{26}$$

The O_2 is consumed by the bacterium in two pathways. The first is due to normal aerobic metabolic activity and the second is due to the bioluminescence reaction. We assume that bacteria can regulate its level of aerobic-anaerobic activity and decrease the level of O_2 consumption correspondingly to the O_2 concentration fitted by $P_{O_2uptake}$ coefficient. Therefore, the change in O_2 molecules available per bacterium could be expressed as follows:

$$\frac{\mathrm{d}O_2}{\mathrm{d}t} = -\left(K_{O_2norm}\left(\frac{O_2(t)}{N_{O_2-b}}\right)^{P_{O_2uptake}} + \frac{N_{photons}(t)}{QE_{luc}}\right), \tag{27}$$

where $N_{photons}$ is the number of photons emitted per $\mathrm{d}t$ time and QE_{luc} is a quantum efficiency of the bioluminescence process.

2.5 Bioluminescence generation process

The bioluminescence generation process implements the reporting part of the biosensor. The detailed description of the process presented in Appendix, while in this section we implement a simplified model, see Fig. 6(b). Bioluminescence generation occurs due to the presence of enzymes generated by lux genes and a number of substrates participating in a "Light Generation Cycle" (LGC), as shown in Fig. 6(a).

The substrates required for the LGC are: (i) energy molecules: ATP, $NADPH$ and $FMNH_2$ along with (ii) other molecules: O_2, H_2O and activated fatty acyl groups ($RCO.ACP$). In this work we assume that substrates are in excess, except for energy molecules and O_2.

There are two groups of the lux related enzymes participating in LGC. The first group is a complex of three enzymes: transferase, synthetase and reductase, presented as triangular in Fig. 6 with letters "t" "s" and "r" correspondingly. The primary function of those enzymes is the generation of luciferin from the substrates. The second group consists of single enzyme luciferase, "l", responsible for the generation of the light emission from the luciferin.

The induction mechanism, indicated by an arrow "Promotion" in Fig. 6(a), is different for each kind of the promoter. For the $recA$ promoter, used in the current work, the promoter activation is repressed by the LexA protein bound to the recA activation site. Therefore, the promotion intensity is a function of the LexA protein concentration in the cell, described in the SOS sub-section. We represent the promotion intensity, I_{Pr}, by the following expression:

$$I_{Pr}(LexA) = I_{Pr-min} + \frac{LexA_{norm} - LexA}{LexA_{norm} - LexA_{min}}, \tag{28}$$

where I_{Pr-min} is the basic promotion intensity and $LexA_{norm}$ is a concentration of LexA for the non-induced state of the biosensor. The $LexA_{min}$ is an experimental parameter taken from the literature [11, 37].

(a)

(b)
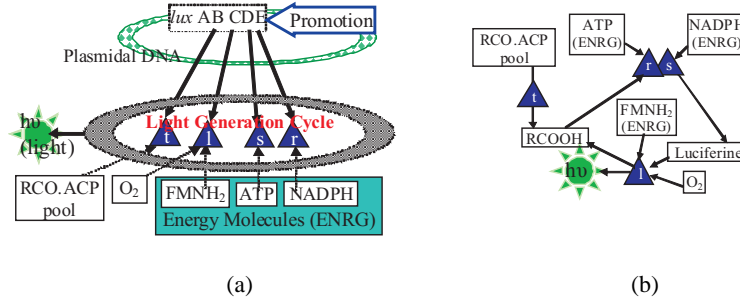
Fig. 6. Bioluminescence reporting part of the bacterial biosensor.

The enzymes are generated through plasmidal DNA transcription and then the translation process. The number of plasmids in the cell, $N_{plasmids}$, is controllable during the biosensor genetical engineering. First, mRNA containing $luxABCDE$ coding sequence is transcribed with the maximal rate of T_c, multiplied by the number of plasmid copies and by the promotion intensity factor. The mRNA concentration, considering the mRNA half-life time H_{RNA}, is expressed by the following differential equation:

$$\frac{\mathrm{d}mRNA}{\mathrm{d}t} = N_{plasmids} \cdot I_{Pr}(LexA) \cdot T_c - \frac{mRNA}{H_{RNA}}. \tag{29}$$

Next, the enzymes are translated by ribosomes moving on the mRNA patterns with an enzymes generation rate of T_l. Enzymes, like all protein molecules, are going through degradation processes and are therefore characterized by a decay rate or half-life time. The luciferase enzyme is considered as a stable protein with half life time H_{sp}, while the transferase, synthetase and reductase are unstable proteins with half life time of H_{up} [38]. The concentrations of the luciferase E_l and reductase, synthetase, transferase $E_{r,s,t}$ are expressed by the following differential equations:

$$\frac{\mathrm{d}E_l}{\mathrm{d}t} = mRNA \cdot T_l - \frac{E_l}{H_{sp}} \quad \text{and} \quad \frac{\mathrm{d}E_{r,s,t}}{\mathrm{d}t} = mRNA \cdot T_l - \frac{E_{r,s,t}}{H_{up}}. \tag{30}$$

The simplified LGC, see Fig. 6(b), consists of enzymes, external inputs, intermediate products and output as photon emission. The intermediate product Fatty Acid (or RCOOH), whose concentration is signed by FA, is created by transferase E_t and luciferase E_l enzymes activity. The Fatty Acid is converted to Luciferine, whose concentration is marked by L, by means of synthetase and reductase enzymes E_{sr}. The conversion process requires also ATP and NADPH energy molecules, whose concentration is signed by $ENRG$. Finally, luciferase converts the Luciferine molecule into photon. This reaction requires also molecular oxygen O_2 and $FMNH_2$ energy molecule.

The change in the concentration of Fatty Acid depends on the reaction constants that relate to transferase, k_t, luciferase, k_l and synthetase-reductase, k_{rs}, activities and Fatty Acid half life time H_{FA}:

$$\frac{\mathrm{d}FA}{\mathrm{d}t} = k_t \cdot E_t + k_l \cdot L \cdot E_l - k_{rs} \cdot FA \cdot E_{r,s} - \frac{FA}{H_{FA}}. \tag{31}$$

The luciferine is generated from the fatty acid in a chain reaction mediated by synthetase and reductase enzymes and also depends on consumption by luciferase and the luciferine half life time, H_{lcfr}:

$$\frac{\mathrm{d}L}{\mathrm{d}t} = k_{rs} \cdot FA \cdot E_{rs} - k_l \cdot L \cdot E_l - \frac{L}{H_{lcfr}}. \tag{32}$$

The k_t reaction coefficient relies on reaction constant $k_{t-basic}$ and also treats the situation where the product is above saturation concentration FA_{sat}:

$$k_t = k_{t-basic} \cdot \frac{FA_{sat}}{FA + FA_{sat}}. \tag{33}$$

The generated product fatty acid is used as a substrate for luciferine product generation mediated by synthetase-reductase, k_{rs}, reaction coefficient. This coefficient is expressed through reaction constant $k_{rs-basic}$, adjusted by substrate saturation concentration FA_{sat}, and availability of the energy molecules:

$$k_{rs} = k_{rs-basic} \cdot \frac{1}{FA + FA_{sat}} \cdot \left(\frac{ENRG}{ENRG_{norm}} \right)^{P_{ENRG}}. \tag{34}$$

The same is for luciferase related reaction coefficient k_l, while it is also adjusted by availability of the molecular oxygen.

$$k_l = k_{l-basic} \cdot \frac{1}{L + L_{sat}} \cdot \left(\frac{ENRG}{ENRG_{norm}} \right)^{P_{ENRG}} \cdot \left(\frac{O_2}{O_{2-norm}} \right)^{P_{O_2}}. \tag{35}$$

The number of the generated photons per unit time is proportional to the k_l constant and number of the luciferine molecules along with luceferase enzyme and quantum efficiency of the light emission QE_{luc}. The number of the emitted photons N_{ph} is expressed in the next manner:

$$N_{photons} = (N_A \cdot V_b \cdot QE_{luc} \cdot k_l \cdot L \cdot E_l) \, \mathrm{d}t. \tag{36}$$

We have expressed a photons emission process that depends on $LexA$, $ENRG$ and O_2 input levels. This section completes the puzzle of modeling the physiological processes of the genetically engineered biosensor described in the current work. Following, it is shown how this model is implemented as a computational program.

3 Numerical implementation of the mathematical model

In this section we show an implementation of the biosensor response mathematical model. First, we show the general technique of the numerical solution using iterations, following reaction constants and initial conditions are presented, and finally the outcomes of the simulations are shown.

3.1 Numerical solution by iterations

We implemented the modules of the mathematical model, described in the previous section, using numerical method. First, we defined interaction step dt and a number of iterations according to the total simulation time requirement T_{sim}, that is usually no longer than 5 hours. Next, we ran loops? of n_{intr} iterations:

$$n_{intr} = T_{sim}/dt. \tag{37}$$

Most equations used in the model are expressed in the form of Ordinary Differential Equation (ODE): $dX(t)/dt = F(X(t))$. In order to implement them numerically, we calculate the change dX for single iteration i, and the value of the X for next iteration – $X(i+1)$:

$$dX = F\big(X(i)\big)dt,$$
$$X(i+1) = \max\big(0, X(i) + dX\big). \tag{38}$$

We have to use $\max(0, X(i) + dX)$ because X represents a concentration or number of molecules that cannot be negative. The precision of the equations solution, as well as run time, is a function of dt value. We found that dt of 1 sec provides a smooth enough solution and reasonable run-time (about $1,000$ iterations per minute on 1.6 GHz PM processor).

3.2 Experimental inputs, initial conditions, reaction coefficients and variables

For conversion of the mathematical model developed in the previous section we need to substitute initial conditions and coefficients for the equations presented there. Parts of the values are available from references. The other part was not found in references and either should be experimentally measured or assumed. In this work missing data was estimated based on expected values and adjusted to yield a good behavior.

In this subsection the values used in the mathematical models are gathered into the tables. First, the experimental inputs are presented in Table 1. Next, intermediate variables are gathered into Table 2. Then we put initial conditions used for the variables into Table 3. After that, we show the fitting coefficients, see Table 4, and finally, rates of synthesis, reaction constants and coefficients are placed into Table 5.

518

Table 1. Experimental inputs

Variable	Description	Values Range	Typical
V_{RC}	Reaction Chamber Volume	0.1 μL : 1 mL	1 μL
C_b	Concentration of biosensors	1e4 : 1e7 b/μL	5e5 b/μL
V_b	Volume of bacterium	$1e-16 : 5e-14$ L	$1e-15$ L
C_{an-ppm}	Concentration of analyte in ppm	0 : 1000 mg/L	
MW_{NA}	Molecular weight of NA analyte		232 g/Mole
D	Diffusion coefficients of water-soluble compounds		$1e-5$ cm^2/sec
$N_{plasmids}$	Number of luminescent plasmids in the cell	1–200	100

Table 2. Variables

Variable	Description	Units
N_b	Number of bacteria inside the reaction chamber	bacteria
$V_{RC/b}$	Volume of reaction chamber per bacteria	L
L_{b2b}	Distance between two adjacent bacteria	μm
$N_{an/b}$	Number of analyte molecules per volume utilized by bacterium	molecules
MW_{an}	Molecular weight of the analyte	g/Mole
k_{trn-NA}	Percentage of molecules transported though membrane per given concentration gradient	%/Δmolecules
NA_{out}	Number of the NA molecules outside bacterium	molecules
NA_{in}	Number of the NA molecules inside bacterium	molecules
$NA_{inMolar}$	Concentration of the NA molecules inside bacterium	M
$GyrA$	Gyrase enzyme concentration	M
$GyrA_{inh}$	Inhibited Gyrase by NA	M
$GyrA_{inhDNA}$	Inhibited Gyrase attached to chromosomal DNA	M
T_{GyrA}	GyrA production rate	M/sec
N_{dim}	Number of dimers on chromosomal DNA	dimers
d$N_{dim-gen}$	Number of created dimers per unit time	dimers
d$N_{dim-rep}$	Number of repaired dimers per unit time	dimers
L_{d2d}	Average distance between dimer to dimer	bp
v_{s-max}	Velocity of DNA polymerase movement on DNA	bp/sec
ssDNA	Single Stranded free DNA fragment inside the cell	M
$RecA$	RecA protein concentration	M
$LexA$	LexA protein concentration	M
$C_{O_2-Molar}$	Concentration of O_2 in Molars	M
N_{O_2-ltr}	Number of O_2 molecules per liter	molecules
N_{O_2-b}	Number of O_2 molecules available per bacteria	molecules
K_{O_2norm}	Normal consumption of O_2	molecules/sec/cell
O_2	Consumption of O_2 as function of O_2 concentration and emission intensity	molecules/sec/cell
I_{Pr}	Promotion coefficient of lux genes expression	Unitless

$mRNA$	Concentration of lux genes related mRNA	M
E_l	Luciferase enzymes concentration	M
$E_{r,s,t}$	Reductase, synthetase, transferase enzymes	M
FA	Faty Acid concentration concentration	M
L	Luciferase concetration	M
k_t	Transferase reaction coefficient as function of FA	$\sec^{-1}$
k_{rs}	Reductase-synthetase reaction coefficient as function of FA, and energy molecules	$(\mathrm{M}\sec)^{-1}$
k_l	Luciferase reaction coefficient as function of L, energy and O_2 molecules	$(\mathrm{M}\sec)^{-1}$

Table 3. Initial conditions

Variable	Description	Value	References
$GyrA_{norm}$	Normal gyrase concentration	$1,000$ molecules	[39]
$GyrA_{min}$	Minimal concentration of gyrase due to regulation	100 molecules	Assumption
$GyrA(0)$	Gyrase concentration at time 0	$GyrA_{norm}$	[39]
$GyrA_{inh}$	Inhibited gyrase concentration at time 0	0 M	Assumption
$GyrA_{inhDNA}$	Inhibited gyrase attached to DNA at time 0	0 M	Assumption
$DNAP$	DNA Polymerase enzymes	20 enzymes	[11]
L_{ChrDNA}	Length of the chromosomal DNA of $E.Coli$	4.72e6 bp	[11]
$RecA(0)$	RecA concentration at time 0	$1.8e-5$ M	[11]
$LexA_{norm}$	LexA concentration in non-induced biosensor	$1.45e-6$ M	[11]
$LexA_{min}$	LexA concentration for maximum induction	$1.45e-7$ M	[11, 37]
$LexA(0)$	LexA concentration at time 0	$LexA_{norm}$	[11]
$ssDNA(0)$	ssDNA concentration at time 0	0 M	Assumption
N_{dim}	Number of dimemrs at time 0	0	Assumption
$Protease(0)$	Protease concentration at time 0	0 M	Assumption
$ENRG_{norm}$	Normal concentration of energy molecules	$1e-3$ M	Assumption
$ENRG(0)$	Energy Molecules at time 0	$ENRG_{norm}$	Assumption
$O_2(0)$	K_{O_2norm}	$40\ \mathrm{amol}/(\mathrm{min\ cell})$	[36]
$mRNA(0)$	mRNA by lux genes expression at time 0	0	Assumption
$E_{l,r,s,t}(0)$	Concentration of lux related enzymes at time 0	0	Assumption
C_{O_2}	Molecular Oxygen (O_2)	9.5 mg/L	[40]
	Tetradecanoyl-ACP (RCO.ACP)	In excess	Assumption
$FA(0)$	Fatty acid ($RCOOH$) at time 0	0 M	Assumption

$L(0)$	Long-chain aliphatic aldehyde or lucefirine ($RCHO$) at time 0	0 M	Assumption
$ENRG_{norm}$	Adenosine tro-Phosphate (ATP)	$1e-3$ M	Assumption
$ENRG_{norm}$	Reducing power ($NADPH$)	$1e-3$ M	Assumption
$ENRG_{norm}$	Reduced Flavin mononucleotide ($FMNH_2$)	$1e-3$ M	Assumption

Table 4. Fitting coefficients (current work assumptions)

Variable	Description	Value
P_{GyrA}	Gyrase production regulation fitting	1
P_{dim}	Fitting energy molecules concentration versus dimers number	1/4
P_{ENRG-v}	Fitting velocity of DNA Polymerase versus $ENRG$ concentration	1/4
P_{ENRG}	Fitting enzyme-substrate reaction coefficient requiring $ENRG$ molecules	1/4
$P_{O_2 uptake}$	Fitting O_2 consumption regulation	2
P_{O_2}	Fitting luciferase reaction coefficient versus O_2 concentration	1/4

Table 5. Rates, constants and coefficient

Variable	Description	Value	Reference
N_A	Avogadro Number	6e23 particles/M	
H_{NA}	Half life time of the NA molecule	$1,500$ sec	Assumption
$k_{GyrA.NA}$	Rate of reaction between NA and gyrase molecules	$1\,(\sec M)^{-1}$	Assumption
k_{dim}	Rate of DNA damage by attached inhibited gyrase	0.01 dim/sec/mlcl	Assumption
$k_{GyrA.DNA}$	Rate of gysrase molecules attachment to DNA	$0.01\,\sec^{-1}$	Assumption
H_{GyrA}	Gyrase half life time	3350 sec	Assumption
$T_{GyrAnorm}$	Normal rate of gyrase synthesis	$0.2985/(N_A\,V_b)$	Assumption
k_{bind}	Binding probability of DNAP to chromosomal DNA	0.5	Assumption
t_{dim}	Time to repair damaged part of the DNA	10 sec	Assumption
v_{s-max}	Velocity of DNA polymerase movement on DNA	1e3 bp/sec	[11]
$k_{protease}$	Rate of RecA and ssDNA transformation to Protease	$6.2e3\,(\sec M)^{-1}$	[11]
H_{ssDNA}	Half life time of ssDNA decomposition	$1e-2\,\sec^{-1}$	Assumption
$H_{Protease}$	Half life time of Protease autodigestion	$1e-3\,\sec^{-1}$	Assumption
$H_{Pr-dcmp}$	Half Protease decomposition time	$9e-3\,\sec^{-1}$	[11]
H_{LexA}	Half life time of LexA autodigestion	$2.18e-4\,\sec^{-1}$	Assumption
T_{LexA}	LexA maximum production rate	$2.323e-8$ M/sec	Assumption
EK_{LexA}	LexA equilibrium constant	$5e7\,M^{-1}$	[11]
H_{RecA}	Half life time of RecA autodigestion	$2.14e-5\,\sec^{-1}$	[11]

T_{RecA}	RecA maximum production rate	$2.79\mathrm{e}-7$ M/sec	[11]
EK_{RecA}	RecA equilibrium constant	5e8 M/sec	[11]
K_{O_2-mol}	Consumption of O_2 in aerobic condition per bacteria	40 amol/(min cell)	[36]
QE_{luc}	Photon emission quantum efficiency	2 %	[41]
I_{Pr-min}	Promotion of lux genes expression at non-induction condition	0.0075	Assumption
T_c	Maximal transcription rate of lux mRNA	$2.5\mathrm{e}-10$ M/sec	[38]
T_l	Maximal translation rate of lux related enzymes	0.25 enz/sec	[38]
H_{RNA}	mRNA half life time	600 sec	Assumption
H_{sp}	Half life time of stable protein	$3,600$ sec	[38]
H_{up}	Half life time of unstable protein	600 sec	[38]
H_{FA}	Half life time of Fatty Acid	100 sec	Assumption
H_{lcfr}	Half life time of Luciferase	1000 sec	Assumption
$k_{t-basic}$	Basic value of transferase - substrate reaction coefficient	$1\mathrm{e}2\ \mathrm{sec}^{-1}$	Assumption
$k_{rs-basic}$	Basic value of reductase-synthetase – Fatty Acid reaction coefficient	$1\mathrm{e}2\ \mathrm{sec}^{-1}$	Assumption
$k_{l-basic}$	Basic value of luciferase – luciferin reaction coefficient	$1\mathrm{e}1\ \mathrm{sec}^{-1}$	Assumption
L_{sat}	Saturation concentration for luciferase	$1\mathrm{e}-2$ M	Assumption
FA_{sat}	Saturation concentration for fatty acid	$1\mathrm{e}-2$ M	Assumption

3.3 Simulation results

In this section we present results of simulation runs of the mathematical model implemented in this work. We used reaction coefficients and initial conditions mapped in the previous section. The simulation input was set according to the experiment presented in the next section and it corresponds to the typical values in Table 1. The following concentrations of the NA analyte were used: 0 ppm, 0.78 ppm, 3.13 ppm, 12.5 ppm, 25 ppm, 50 ppm and 100 ppm.

At the first stage the simulation takes the biosensors to the steady state. This steady state emulates preparation of the biosensors under ideal incubating conditions without limit in O_2, nutrients and absence of toxic materials in the medium. The process lasts about 150 minutes. The luminescence reaches a stable base level making it possible to pass to the second stage of simulation, where the biosensors are encapsulated into the observation chambers without additional O_2 and nutrients supply and are challenged with various concentrations of the NA analyte.

The simulation results for the second stage are presented in Figs. 7, 8. Each figure contains sub-plots exhibiting kinetics of components used in the model. The components are identified according to the title on the top of the sub-plot. The first, Fig. 7, shows results of the SOS process; while the second, Fig. 8, demonstrates kinetics of the light generation cycle. The x-axis for each sub-plot is time in minutes.
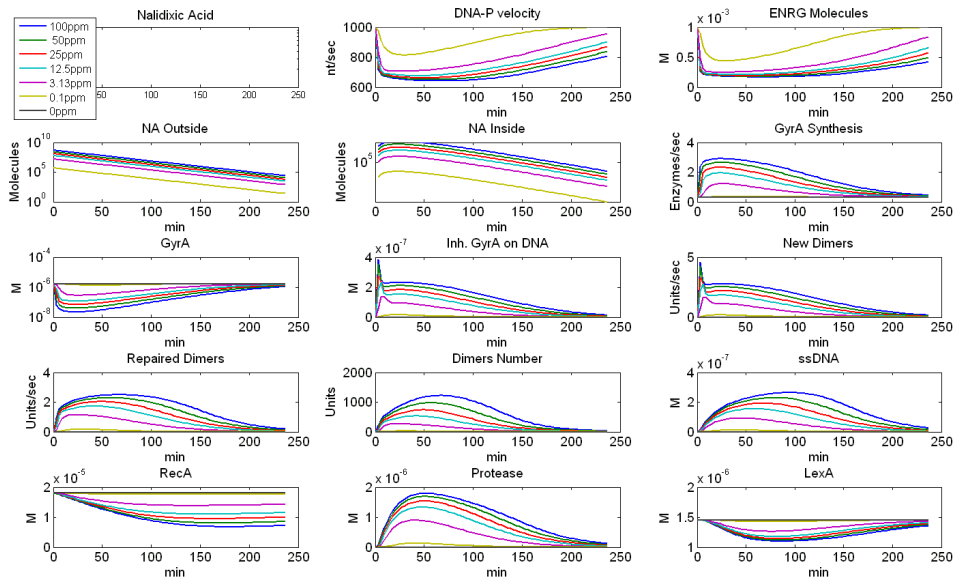
Fig. 7. Simulation results: SOS process.
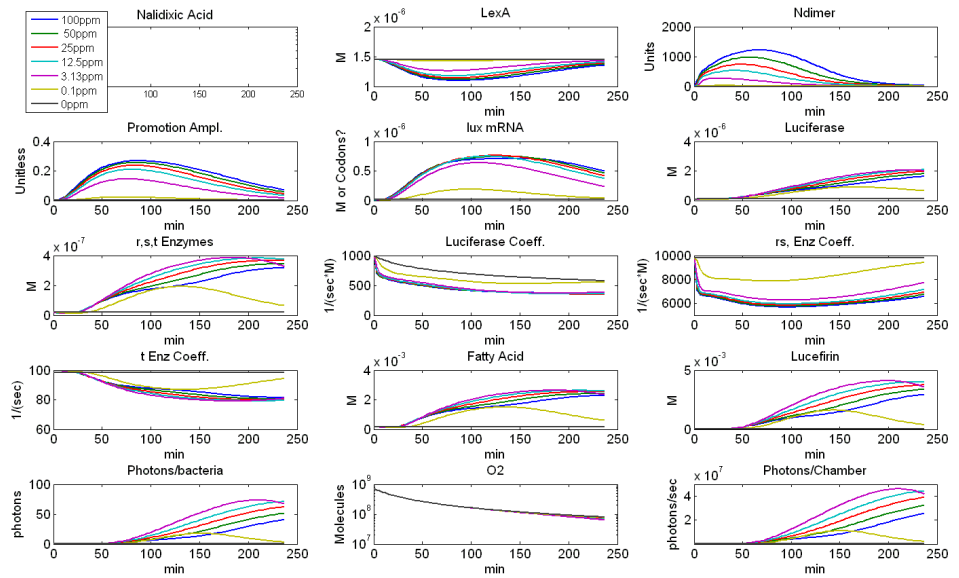
Fig. 8. Simulation results: light generation cycle.

In the next section actual results for the same Nalidixic Acid concentrations, as in simulations, are presented and compared. The experimental results contain only kinetics of emission intensity versus time. Therefore it is extremely challenging to analyze bottlenecks for experimental results, while, as could be seen from this section, using simulation is very friendly.

4   Experimental results and discussions

4.1   The experimental setup

The measurements were performed on a Victor-II luminometer by Wallac Inc. using a 384 chambers microtiter plate. To avoid cross-lighting, each second chamber was utilized for the experiment. The working chambers were fully filled by a solution containing Luria Bertani (LB) medium, bacteria under concentration of $5e8$ bacteria/mL and different concentrations of Nalidixic Acid (NA). The working chamber volume is about 50 μL, and therefore included about $2.5e7$ bacteria. The top of the microtirtle plate was sealed by a transparent film to avoid oxygen supply (in order to emulate biochip condition). We used the following NA concentrations: 0 ppm, $0.1, 3.13, 12.5, 25, 50, 100$ ppm. In addition, chambers with water only and with water and LB only were prepared. Four repetitions were set up for every NA concentration. The light intensity from the each reaction chamber was sampled once in 3 minutes.

4.2   Experimental results

The experimental results are demonstrated in Fig. 9. The y-axis is the total collected light intensity in [photons/sec] units and the x-axis is the time since analytes intervention in minutes. There is an individual curve for each NA concentration. The experiment was performed during 240 minutes similarly to the time of the simulation.

4.3   Discussions

As can be seen, the kinetics of simulation matches quite reasonably the experimental results (see Fig. 10 and Fig. 9). The biosensors are in Stress, Metabolic Recovery and SOS states (see Section 2.1) for the first 45 minutes. The luminescence intensity reaches the same order of magnitude $1e7$ [photons/sec] during the "Response State" and finally the luminescence activity discards after about 180 minutes correspondingly to the reversion of the biosensor to the "Idle State". Even though the kinetics as a function of NA concentration did not match precisely, the main goal of the current work, Stage-I, has been achieved (see Fig. 1 in Section 1). We still have to note that the quality of results during the Stage-II can't be fully estimated. This is due to complexity of the presented model from one side and simplifications of the biological processes from the other, as well as possibility of non-unique solutions for the fitting of experimental data.
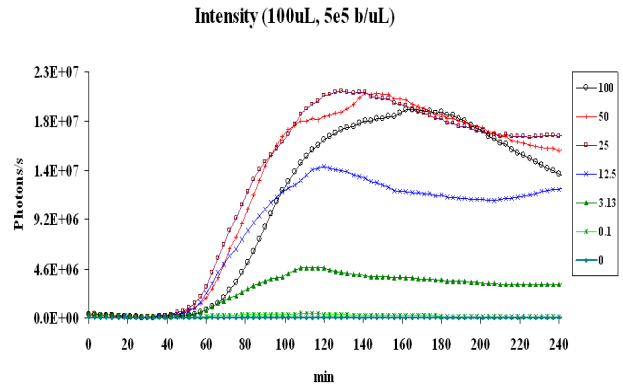
Fig. 9. Experimental results.
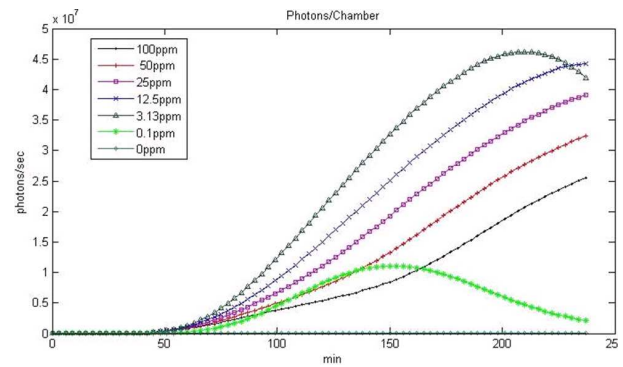
Fig. 10. Simulation results: light intensity vs. NA concentration.

5   Conclusions

In this work we have presented a design of the mathematical model of the response of a whole cell based biosensor, as well as simulation results generally matching the simulation. We have defined the three stages for implementation of Biological Computer Aided Design (bio-CAD) software and successfully fulfilled the first stage. The completion of the next two stages would require collaborative work of (i) bio-mathematical modeling; (ii) molecular biologists; and (iii) engineers. This extremely challenging task, considering obstacles such as complexity of the model and non-unique solutions for the inverse problems and may demand 10 to 20 man years of R&D. However, once the bio-CAD software would be available, the development of the whole cell based biosensors will be boosted in a few orders of magnitude.

Appendix. Comprehensive model of light generation cycle

In this appendix the information from the prior-works [5, 30, 31, 42] is integrated into a comprehensive LGC chemical and mathematical model. This process is illustrated in the chart below. The lux enzymes E_l, E_r, E_t and E_s are generated by corresponding genes $luxAB, C, D, E$ with the generation rates k_{AB}, k_C, k_D and k_E. Those generation rates are different to each gene and have units of [M/sec/Pr]. The enzymes are marked by a triangular shape. The enzymes are also having half life time constants $k_{e0.5\tau}$. The transaction between the reactions compounds are accompanied with the chemical reaction rate constant k_{rate} (see Table below). Part of the reactions are reversible and their constants are marked k_{-rate} correspondingly.
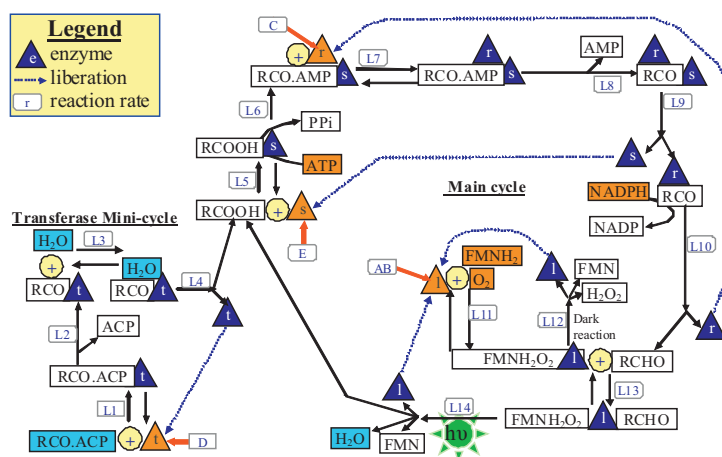
The names of molecules participating in the LGC are presented in the Table:

Formula	Instance	Formula	Instance
$RCO.ACP$	Tetradecanoyl-ACP	$RCO.E_r.E_s$	Tetradecanoyl Synthesaze – Reductase complex
$RCO.ACP.E_t$	Tetradecanoyl-ACP-transferase intrmediate	$RCO.E_r$	Tetradecanoyl Reductase complex
$RCO.E_t$	Cleaved Tetradecanoyl	$NADPH$	Reducing power
ACP	Acyl carrier protein	$RCHO$	Luciferine or Aldehide
$RCO.H2O.E_t$	Cleaved Tetradecanoyl intermediate with water	$FMNH2O_2.E_l$	Flavin oxiginated luciferase intermediate
H_2O	Water	$FMNH_2O_2.$ $E_l.RCHO$	Flavin oxiginated aldehide luciferase intermediate
RCO	Fatty acid residue	$FMNH_2$	Reduced Flavin mono-nucleotide

$RCOOH$	Fatty acid	FMN	Flavin mononucleotide
$RCOOH.E_s$	Fatty acid intermediate with Synthesaze	O_2	Molecular Oxygen
$RCO.AMP$	Fatty Acyl-AMP	$RCHO$	Long-chain aliphatic aldehyde or lucefirine
$RCO.AMP.$ $E_r.E_s$	Fatty Acyl-AMP Synthesaze – Reductase complex		

References

1. A. Antoniotti et al., Taming the complexity of biochemical models through bisimulation and collapsing: theory and practice, *Theor. Comput. Sci.*, **325**(1), pp. 45–67, 2004.

2. C. F. Mandenius, Recent developments in the monitoring, modeling and control of biological production systems, *Bioprocess and Biosystems Engineering*, **26**(6), pp. 347–351, 2004.

3. J. Stelling, Mathematical models in microbial systems biology, *Curr. Opin. Microbiol.*, **7**(5), pp. 513–518, 2004.

4. R. Alur et al., Modeling and analyzing biomolecular networks, *Comput. Sci. Eng.*, **4**(1), pp. 20–31, 2002.

5. K. Salama et al., Modeling and simulation of luminescence detection platforms, *Biosens. Bioelectron.*, **19**(11), pp. 1377–1386, 2004.

6. A. Zaslaver et al., Just-in-time transcription program in metabolic pathways, *Nat. Genet.*, **36**(5), pp. 486–491, 2004.

7. A. Neykov, V. Rangelova, Mathematical modeling of the biosensor systems, *Biotechnol. Biotec. Eq.*, **12**(2), pp. 100–109, 1998.

8. R. Daniel et al., Modeling and measurement of a whole-cell bioluminescent biosensor based on a single photon avalanche diode. *Biosens. Bioelectron.*, **24**(4), pp. 882–887, 2008.

9. R. Baronas, J. Kulys, F. Ivanauskas, Mathematical model of the biosensors acting in a trigger mode, *Sensors*, **4**, pp. 20–36, 2004.

10. S. James et al., Luminescence control in the marine bacterium Vibrio fischeri: An analysis of the dynamics of lux regulation, *J. Mol. Biol.*, **296**(4), pp. 1127–1137, 2000.

11. S. V. Aksenov, E. A. Krasavin, A. A. Litvin, Mathematical model of the SOS response regulation of an excision repair deficient mutant of Escherichia coli after ultraviolet light irradiation, *J. Theor. Biol.*, **186**(2), pp. 251–260, 1997.

12. S. V. Aksenov, Induction of the SOS response in ultraviolet-irradiated Escherichia coli analyzed by dynamics of LexA, RecA and SulA proteins, *J. Biol. Phys.*, **25**(2–3), pp. 263–277, 1999.

13. S. V. Aksenov, Dynamics of the inducing signal for the SOS regulatory system in Escherichia coli after ultraviolet irradiation, *Math. Biosci.*, **157**(1–2), pp. 269–286, 1999.

14. D. Holcman, Z. Schuss, Stochastic chemical reactions in microdomains, *J. Chem. Phys.*, **122**(11), 2005.

15. A. Hassibi et al., Biological shot-noise and quantum-limited signal-to-noise ratio in affinity-based biosensors, *J. Appl. Phys.*, **97**(8), 2005.

16. J. Puchalka, A. M. Kierzek, Bridging the gap between stochastic and deterministic regimes in the kinetic simulations of the biochemical reaction networks, *Biophys. J.*, **86**(3), pp. 1357–1372, 2004.

17. B. Palsson, Metabolism: a bird's eye view, `http://gcrg.ucsd.edu/classes/1/_2/_metabolism.pdf`, 2002.

18. J. McMurry, T. Begley, Nucleotide metabolism, in: *The Organic Chemistry of Biological Pathway*, pp. 305–227, 2004.

19. M. Thattai, B. I. Shraiman, Metabolic Switching in the Sugar Phosphotransferase System of Escherichia coli, *Biophys. J.*, **85**(2), pp. 744–754, 2003.

20. S. Holzhutter, H. G. Holzhutter, Computational design of reduced metabolic networks, *ChemBioChem*, **5**(10), pp. 1401–1422, 2004.

21. W. Boos, H. Shuman, Maltose/maltodextrin system of escherichia coli: transport, metabolism, and regulation, *Microbiol. Mol. Biol. R.*, **62**(1), pp. 204–229, 1998.

22. L. Cournac et al., Sustained photoevolution of molecular hydrogen in a mutant of synechocystis sp. strain PCC 6803 deficient in the type I NADPH-dehydrogenase complex., *J. Bacteriol.*, **186**(6), pp. 1737–1746, 2004.

23. D. E. Nivens et al., Bioluminescent bioreporter integrated circuits: potentially small, rugged and inexpensive whole-cell biosensors for remote environmental monitoring, *J. Appl. Microbiol.*, **96**(1), pp. 33–46, 2004.

24. J. R. van der Meer, D. Tropel, M. Jaspers, Illuminating the detection chain of bacterial bioreporters, *Environ. Microbiol.*, **6**(10), pp. 1005–1020, 2004.

25. T. S. Gardner et al., Inferring genetic networks and identifying compound mode of action via expression profiling, *Science*, **301**(5629), pp. 102–105, 2003.

26. M. D. Sutton et al., The SOS response: recent insights into umuDC-dependent mutagenesis and DNA damage tolerance, *Annu. Rev. Genet.*, **34**, pp. 479–497, 2000.

27. N. Yildirim, M. C. Mackey, Feedback regulation in the lactose operon: a mathematical modeling study and comparison with experimental data, *Biophys. J.*, **84**(5), pp. 2841–2851, 2003.

28. R. Bundschuh, F. Hayot, C. Jayaprakash, Fluctuations and slow variables in genetic networks, *Biophys. J.*, **84**(3), pp. 1606–1615, 2003.

29. E. N. Harvey, The total luminous efficiency of luminous bacteria, *J. Gen. Physiol.*, **8**(2), pp. 89–108, 1925.

30. C. J. Kelly, C.-J. Hsiung, C. A. Lajoie, Kinetical analysis of bacterial bioluminescence, *Biotechnol. Bioeng.*, **81**, pp. 370–378, 2003.

31. J. Lee , C. L. Murphy, Bacterial bioluminescence: equilibrium association measurements, quantum yields, reaction kinetics, and overall reaction scheme, *Biochemistry*, **14**(10), pp. 2259–2268, 1975.

32. I. V. Sokolova, G. S. Kalacheva, N. A. Tyulkova, Analysis of the ration of quantum yield and fatty acid formation of photobacterium leiognathi bioluminescence. *Vestnik moskovskogo universiteta. Khimiya*, **41**(6), pp. 118–120, 2000.

33. K. G. Newmark et al., Genetic analysis of the requirements for SOS induction by nalidixic acid in Escherichia coli. *Gene*, **356**, pp. 69–76, 2005.

34. P. R. Jensen et al., Extensive regulation compromises the extent to which DNA gyrase controls DNA supercoiling and growth rate of Escherichia coli, *European Journal of Biochemistry*, **266**(3), pp. 865–877, 1999.

35. A. Rabner et al., Whole-cell luminescence biosensor-based lab-on-chip integrated system for water toxicity analysis, in: *Microfluidics, BioMEMS, and Medical Microsystems IV*, Proceedings of the SPIE, Vol. 6112, pp. 33–42, 2006.

36. J. J. Bourgois et al., Kinetics of light emission and oxygen consumption by bioluminescent bacteria, *J. Bioenerg. Biomembr.*, **33**(4), pp. 353–363, 2001.

37. M. Takahashi, M. Schnarr, Investigation of reca polynucleotide interactions from the measurement of lexa repressor cleavage kinetics – presence of different types of complex, *Eur. J. Biochem.*, **183**(3), pp. 617–622, 1989.

38. C. Belta et al., *Stability and reachability analysis of a hybrid model of luminescence in the marine bacterium Vibrio fischeri*, technical report.

39. Z. H. Pang et al., A gyrase mutant with low activity disrupts supercoiling at the replication terminus, *J. Bacteriol.*, **187**(22), pp. 7773–7783, 2005.

40. BPA, Dissolved oxygen fact sheet, `http://www.bpa.gov/Corporate/KR/ed/kidsinthecreek/topics/waterquality/do.htm`.

41. J. C. Makemson, Luciferase-dependent oxygen-consumption by bioluminescent vibrios, *J. Bacteriol.*, **165**(2), pp. 461–466, 1986.

42. G. B. Zavilgelsky et al., Role of Hsp70 (DnaK-DnaJ-GrpE) and Hsp100 (ClpA and ClpB) chaperones in refolding and increased thermal stability of bacterial luciferases in Escherichia coli cells, *Biochemistry-Moscow+*, **67**(9), pp. 986–992, 2002.